Impact of Model Differences in Quantitative Analysis of FUV Auroral Emissions: Total Ionization Cross Sections

G. A. Germany[1], D. Lummerzheim[2], and P. G. Richards[3]

Received _____; accepted _____

Submitted to the *Journal of Geophysical Research -- Space Physics*, 2000.

Short title: IMPACT OF CROSS SECTIONS

[1] Center for Space Plasma & Aeronomic Research, University of Alabama in Huntsville, S131 Technology Hall, Huntsville, AL 35899

[2] Geophysical Institute, University of Alaska, Fairbanks AK

[3] Computer Science Department, University of Alabama in Huntsville

Abstract

A sensitivity study was performed in which the peak height of modeled FUV auroral emissions was displaced in altitude, an effect that can result from several causes in the modeling process. The purpose of the study was to examine the impact of such displacements on energy parameters extracted from FUV auroral observations. For this study, the N_2 total ionization cross section was modified above 1 keV. Cross section modifications are investigated for a variety of reasons including the fact that they can directly impact modeled emission height profiles and because different cross section sets are adopted by different modelers. Though physically unrealistic, the magnitude of the change in cross section considered here is large enough that this study covers the expected range of uncertainties within a single model, or between two or more different models. The values reported here can thus be viewed as upper limits for these uncertainties. The high energy modifications result in changes of up to 3 km in the altitude of peak emission for FUV emissions excited by 10 keV electrons. For calculations using data from the Polar Ultraviolet Imager, derived energy flux and mean energy are changed by up to 16% and 23%, respectively, for 10 keV incident electrons.

1. Introduction

Far ultraviolet (FUV) images of the Earth's aurora as seen from space are finding increased use in morphological, synoptic, and correlative studies [e.g. *Anderson et al.*, 2000; *Brittnacher et al.*, 1999; *Germany et al.*, 1998c; *Germany et al.*, 1998b; *Chua et al.*, 1998; *Angelopoulos et al.*, 1997; *Liou et al.*, 1997], as well as quantitative studies based on photometric analysis of auroral intensities [*Ostgaard et al.*, 2000; *Germany et al.*, 1998a; *Germany et al.*, 1997; *Lummerzheim et al.*, 1997; *Doe et al.*, 1997]. The latter studies have focused heavily on the estimation of auroral energy parameters (principally total energy flux and mean energy) because of their importance in mapping energy flow between the magnetosphere and the ionosphere, as well as being precursors to ionospheric conductivity calculations. Energy analysis of FUV auroral emissions is based upon energy-dependent loss mechanisms, primarily absorption by O_2 [e.g. *Strickland et al.*, 1983], and has been discussed elsewhere [*Germany et al.*, 1990; *Germany et al.*, 1994b; *Germany et al.*, 1994a; *Lummerzheim et al.*, 1991]. In brief, the principal loss mechanism for FUV photons viewed from space is wavelength-dependent absorption within the O_2 Schumann-Runge (SR) absorption continuum. By observing at multiple wavelengths, these differences can be exploited to estimate the altitude of the observed emissions which, in turn, can be used to estimate the energy of the incident auroral particle flux.

Quantitative comparisons between models and observations require a knowledge of the uncertainties associated with both model and measurement. For parameters derived

from observations, e.g. energy derived from FUV images, the error in the derived parameter includes that of the modeling process. Unfortunately, estimating model errors can be a difficult task and simply compiling uncertainties in model inputs can lead to unrealistically high error estimates.

Sensitivity studies in which model parameters are perturbed in a controlled (though not necessarily physically realistic) fashion offer some of the best techniques to assess model dependencies. For FUV observations, model perturbations that affect the modeled emission altitude are very useful, since the absorption loss process for line-of-sight observations is an exponential one which varies rapidly over a relatively small altitude region. Thus small changes in the modeled emissions within this region, particularly the peak emission height, may have larger than expected changes on parameters derived from these emissions.

The goal of this study is to perturb model parameters sufficiently to produce small changes in the altitudes of modeled FUV emissions and then examine energy parameters derived from these emissions. Ideally, the model perturbations would be as limited as possible and would be representative of likely uncertainties in all modeling processes.

A number of factors, e.g. different neutral density models, can affect the height of modeled emissions. For example, *Peticolas and Lummerzheim* [2000], modeling time-dependent electron transport, show that even elastic scattering can affect the altitude of modeled emissions. (See Figure 1 of Peticolas and Lummerzheim.) However, this study is limited to modifying a key model cross section, the total ionization cross section of N_2. Cross sections are investigated because they represent the major source of model uncertainties, because they can directly impact modeled emission heights without the

necessity of modifying the model atmosphere, because they are easily modified, and because different cross section sets are adopted by different modelers. Details of electron transport calculations depend on the particular set of cross sections selected and uncertainties in the cross section selection directly affect modeled emissions. (See, for example, *Lummerzheim and Lilensten* [1994] in which they examine results using two sets of model cross sections.)

It is important to note at this point that the cross section modifications presented below are used solely to produce the desired effects, i.e. changing the modeled emission heights, and are not offered as substitutes for currently accepted cross section parameterizations.

In the sections below, models and cross sections relevant to this study are first discussed. Then the details of the sensitivity study are reported. This is then discussed in the context of analysis of images from the Ultraviolet Imager [*Torr et al.*, 1995].

2. Modeling FUV emissions

The principal loss mechanism for FUV photons viewed from space is absorption within the O_2 Schumann-Runge (SR) absorption continuum between approximately 130 and 175 nm. This absorption is dependent on wavelength and is also a function of the column density of O_2 between the local production region and the observer. For downward-looking space-based viewing geometries this is a strong function of the O_2 altitude distribution. Since the absorption cross section is both wavelength and altitude dependent, the line-of-sight O_2 absorption may be discussed in terms of the column transmission to space (CTS)--defined to be the relative fraction of photons from a given

altitude that can be detected from space--for a selection of FUV emissions. CTS is basically an altitude-dependent attenuation factor that varies with wavelength such that for no O_2 absorption CTS=1, i.e. all photons escape to space, and for total O_2 absorption CTS=0, i.e. all photons are absorbed locally and none are visible from above the atmosphere.

Figure 1 shows CTS functions for 5 bands of the N_2 Lyman-Birge-Hopfield (LBH) band system selected to span the wavelength region between 145.0 and 173.6 nm. The LBH band system is routinely used for auroral energy analysis because it includes emissions within the SR absorption region as well as emissions at longer wavelengths. A typical analysis will compare intensities obtained from LBH bands within the SR absorption region (LBH short) to the intensities of the LBH bands lying longward of this region (LBH long) and thus not experiencing significant O_2 absorption [*Strickland et al.*, 1983; *Germany et al.*, 1990].

For longer wavelength LBH bands, e.g. 173.6 nm in Figure 1, CTS is virtually unity at all altitudes. Hence no significant absorption is encountered and all upward emitted photons can escape to space. At these wavelengths, model uncertainties that result in shifted emission altitudes will have little impact on the total integrated line-of-sight intensity.

For shorter wavelength LBH bands, e.g. 145.0 nm, there is a pronounced change in O_2 attenuation with altitude. In fact, as shown in Figure 1b, the attenuation at 145.0 nm changes by almost two orders of magnitude between 105 and 110 km, the region where auroral emissions produced by 10 keV electrons peak. At these wavelengths, model uncertainties that shift the emission altitude by only a few kilometers will significantly

change the observed line-of-sight intensity. Thus long wavelength LBH emissions are relatively unaffected by model uncertainties while short wavelength emissions are more significantly affected. Energy parameters derived from a comparison of these emissions will clearly be affected as well. The magnitude of these changes is addressed below.

The work presented here uses the two-stream auroral degradation model of *Richards and Torr* [1990], referred to below simply as AURCODE. This code has demonstrated excellent agreement with more detailed multistream models. The results presented here are thus applicable to other auroral modeling efforts as well as those that use the AURCODE algorithm.

Cross sections responsible for the greatest energy loss in the transport calculation are most likely to impact the altitude distribution of the auroral emissions. *Richards and Torr* [1990] examined the partitioning of a 1 mW m^{-2} incident energy flux as a function of energy. Their Figure 4 shows the partitioning of the incident energy flux into excitations, ionizations, and backscattered flux (dotted line). The principal energy sink is the ionization of N_2, accounting for ~35% of the total energy deposited into the thermosphere. Excitation of N_2 is the second largest sink (~20%) and approximately 16% of the initial energy is lost through escaping backscattering flux. All other sources are of considerably less importance. Because the largest partition fraction is controlled by a single cross section, the total ionization cross section of N_2, this study is limited to perturbations in that cross section.

3. Cross Sections

The principal measurements of the total N_2 ionization cross section are over 35 years old, in particular the work of *Rapp and Englander-Golden* [1965]. However the Rapp and Englander-Golden measurements are still considered valid and used in some form by most modelers. *Van Zyl and Pendleton* [1995] recently examined a variety of cross-section data for electron-impact ionization of N_2 at 100 eV, the nominal peak of the total ionization cross section. They tabulated values for the N_2^+ production cross section, which is not the same as the total ionization cross section investigated below. In addition to the production of N_2^+ reported by Van Zyl and Pendleton, electron excitation also creates other ionization products such as atomic ions and doubly ionized states. The total ionization cross section modified in this study corresponds to the total production of all ionization products and is larger than the Van Zyl and Pendleton values. They concluded that consensus measurements of total N_2^+ production are consistent with the *Rapp and Englander-Golden* [1965] measurements, with the total N_2^+ production cross section reported by them representing approximately 73% of the total ionization cross section.

Unfortunately, the Rapp and Englander-Golden measurements only extend to 1 keV while auroral degradation calculations are needed at significantly higher energies. *Schram et al.* [1964] measured the total ionization cross section at energies extending up to 10 keV thereby overlapping the higher energy values of *Rapp and Englander-Golden* [1965]. However, the Schram et al. measurements are significantly smaller than the Rapp and Englander-Golden values in the overlap region near 1 keV. Because of this discrepancy, cross section parameterizations typically use the cross sections of *Rapp and*

Englander-Golden [1965] for energies below 1 keV, with extrapolation of these values to higher energies.

Figure 2 shows measurements and parameterizations of the total ionization cross section for N_2. The measurements of *Rapp and Englander-Golden* [1965] and *Schram et al.* [1964] are shown by circles and crosses, respectively. (The placement of the circles and crosses are estimated from Figure 14 of *Kieffer and Dunn* [1966] and nominal plotting errors of a few percent can be expected.) The error bar at 100 eV represents the (symmetric) 1 standard-deviation range of values adopted from Table 1 of *Van Zyl and Pendleton* [1995] ($26.3 \pm 2.6 \times 10^{-17}$ cm^2). The Van Zyl and Pendleton values have been scaled to convert from N_2^+ production cross section to total N_2 ionization cross section. Table 1 of Van Zyl and Pendleton includes results from 5 studies and a consensus value based on 6 additional studies. The total collection of studies covers results from 1965 to 1995. The error bar thus represents the range of other measurements over the 35 years since the original Rapp and Englander-Golden measurements.

Also shown in Figure 2 are parameterizations of these measurements used by models to allow calculations at energies other than those measured. The first parameterization is from *Strickland and Meier* [1982] (dashed line). This parameterization is widely used and duplicates the *Rapp and Englander-Golden* [1965] measurements well while overstating the *Schram et al.* [1964] value by 35% at 10 keV. AURCODE uses a similar parameterization, but with a larger high energy extrapolation. Recently, a coding error was found in the AURCODE parameterization that resulted in an overestimate of the actual cross section by about 12%. The solid line in Fig 3 shows the AURCODE

parameterization of *Richards and Torr* [1990] with this 12% coding error corrected, hereinafter referred to as the GLR00 parameterization.

The GLR00 extrapolation is based, in part, on measurements of the 3914 N_2^+ excitation cross section by *Borst and Zipf* [1970]. They measured the excitation cross section from threshold to 3 keV and extrapolated data to 10 keV using a Bethe-Oppenheimer relation Q = A ln(BE)/E fitted to observations between 0.2 and 3 keV. The GLR00 parameterization fitted the same relation to the Rapp & Englander-Golden data below 1 keV to determine the high energy dependence. The triangles in Figure 2 show the Borst and Zipf measurements (their Table 1) for energies above 500 eV. The Borst and Zipf values have been normalized to the GLR00 cross section at 1 keV since the 3914 N_2^+ cross section they measured is proportional to the total ionization cross section.

The final parameterization in Figure 2 (dotted line) is one in which the GLR00 parameterization has been modified to more closely match the Schram et al. values above 1 keV. This parameterization will be referred to as TST hereinafter to indicate its temporary, test status for this investigation. Since these two parameterizations (GLR00 and TST) bracket both available measurements and commonly used parameterizations, comparing these two represents an examination of the largest expected uncertainty either within a single model or between different models. These parameterizations are also compared with the original one of *Richards and Torr* [1990] to estimate the extent of the error introduced by the recently corrected coding error. The *Richards and Torr* [1990] parameterization will be referred to as RT90 in the discussion below.

(A brief summary of nomenclature used throughout this paper: RT90, original parameterization used in AURCODE; GLR00, correction of RT90; TST, perturbation considered in this study.)

4. Sensitivity Study

A 10 keV Gaussian energy distribution with an energy flux of 1 mW m^{-2} incident at the top of the model atmosphere was modeled. By 100 km, the downward fluxes from all sources (incident distribution and secondary population) are negligible.

Similar flux calculations were performed for the GLR00 and TST cross section parameterizations. They were then compared by calculating the ratio of downward fluxes from the two parameterizations. The two sets of fluxes are virtually identical (ratio ~1) for altitudes above 120 km. However, at altitudes below 120 km there is significantly increased flux when using the TST parameterization. The overall impact of modifying the cross section parameterization is thus to increase the amount of auroral flux below 120 km and subsequently to increase production of auroral emissions at these altitudes. This is an important point since it is the emitted photons, and not electron fluxes themselves, that are monitored in remote sensing applications. Since there are no significant changes in particle fluxes between the two calculations above 120 km, only auroral emissions from electrons with energies high enough to penetrate below 120 km will be affected. Lower energy emissions will be unaffected.

Figure 3 shows calculated volume production rates for the N_2 ($a^1\Pi_g$) LBH parent state for incident Gaussian distributions with a mean energy of 10 keV. The incident energy flux is 1 mW-m^{-2} in all cases. The TST parameterization (dashed line) is about 3

km lower than either the GLR00 (solid line) values. For lower energies, e.g. 500 eV, both parameterizations produce the same results (not shown). This is consistent with the discussion above that showed modified fluxes only at the lower altitudes.

Also shown in Figure 3 are volume emission rate profiles for O(^{5}S) 135.6 nm under the same conditions as the LBH calculations. (Since the $a^1\Pi$ states emit promptly, the LBH volume production rate is equivalent to its emission rate, except that the emitted energy must be partitioned among each of the individual LBH bands.) The 135.6 nm emission exhibits the same behavior as the LBH calculations, i.e. decreased altitude and magnitude of peak production with the TST parameterization.

Thus the choice of cross section parameterization affects modeled emission parameters on an energy-dependent basis. The central question of this study is thus whether the relatively small changes shown in Figure 3 translate into significant changes in the column-integrated emissions used in remote-sensing missions. In particular, the effects of interactions between the peak height and O_2 absorption must be separated from the decreases in peak production also evident in the figures.

To investigate this latter point further, vertically integrated brightnesses were calculated for the production rate profiles in Figure 3. The calculations were performed both with the effects of local O_2 absorption included and without the absorption process. The relative change in vertical brightness between the GLR00 and TST parameterizations was then compared with the change in peak emission rate.

The results are summarized in Table 1. (Two LBH bands--146.4 and 183.8 nm--are chosen to represent the LBH long and short regions.) With O_2 absorption present, significant changes in column brightness are seen for each of the three emissions, ranging

from about 9 to 71% with emission feature. For the short wavelength emissions (135.6 and 146.4 nm) this is considerably larger than the change in peak emission rate (shown in the second row of the table) while the long wavelength 1838 emission change is on the same order as the change in peak emission rate. However, with absorption disabled, the column brightness changes for all three emissions are essentially the same as the changes in peak emission rate. Thus the majority of the change seen for short wavelength emissions is due to variations in O_2 absorptive loss resulting from the ~3 km change in peak altitude.

As seen in Figure 1, however, the magnitude of this effect varies dramatically with wavelength. The question to be considered thus hinges on the wavelength regions probed in the remote sensing application. As a concrete example, the impact of these changes on data collected from the Ultraviolet Imager and analyzed to extract total energy flux and mean energy will now be examined.

5. Application to UVI observations

The POLAR Ultraviolet Imager (UVI) [*Torr et al.*, 1995] provides auroral images using two filters dedicated to the LBH long and short spectral regions, labeled LBHL and LBHS, respectively. The LBHS filter is centered near the SR peak absorption while the LBHL filter is placed in a region of significantly less absorption. However, due to manufacturing constraints, the LBHL filter includes several bands that have significant O_2 absorption. Thus the UVI LBHL response with energy will share some characteristics with the LBHS filter.

Column brightnesses were calculated by integrating the LBH bands passed by the two filters as a function of incident energy using a Gaussian energy distribution with a 1 mW m^{-2} energy flux was used. While other distributions, e.g. Maxwellian, are more appropriate under some conditions, the choice of distribution does not affect the discussion here. Furthermore, the Gaussian, unlike the Maxwellian, has the distinction of having equal characteristic and mean energies.

The TST cross section significantly decreases both the modeled LBHL and LBHS emissions (not shown) with the relative decrease in LBHS intensity being greater than that in LBHL (16% versus 40%, respectively, at 10 keV). Therefore, the ratio of the LBH emissions is changed with the use of the TST cross section (Figure 4). It is evident that the energy associated with an observed emission ratio will be smaller for TST than for GLR00. The relative change in derived energy for each of the cross section parameterizations is shown in Figure 5. The GLR00 cross section is taken as the reference value and the other curves show how much the derived energy would be changed with the choice of cross section parameterization. For example, an emission ratio that would yield an energy of 10 keV using the RT90 cross section will result in an estimate of approximately 7.7 keV using the TST values. The RT90 cross section yields energy estimates approximately 5% higher than the GLR00 estimates.

In summary, changing the total ionization cross section in the manner discussed above reduces the derived energy flux by about 16% (since the energy flux is directly proportional to the LBHL intensity) and the derived mean energy by almost 23% for 10 keV electrons. The changes are functions of energy and are much smaller at lower energies.

This is comparable to other uncertainties in the UVI analysis. For example, the instrument calibration has an uncertainty on the order of 25%, as is the uncertainty in the LBH cross sections. Additional errors are difficult to characterize such as the change in auroral brightness during the 37 second integration period of UVI, but they are expected to be at least as large.

6. Impact on Other Emissions

This study has focused exclusively on derived energy parameters from LBH emissions and the impact on these parameters of modifications in the total N_2 ionization cross section. The primary goal has been to determine the relative sensitivity of the derived parameters to the cross section, not to justify the choice of cross section. If the goal of this study were to select an improved, or 'best', cross section parameterization for modeling then it would be appropriate to examine a variety of modeled emissions and compare them with observations and other models. In particular, both FUV and visible emissions would be examined since the latter have been the subject of extensive investigation.

Richards and Torr [1990] performed these comparisons and obtained excellent agreement with observations and multistream models, using the RT90 N_2^+ ionization cross sections. Figure 6 shows column intensity versus energy for selected emissions in the FUV and visible (N_2 3371, N_2^+ 3914, O 1356, and LBH 1325) which were previously used as comparison benchmarks with the RT90 cross sections.

As demonstrated in Figure 3, the FUV emissions are significantly reduced and the reduction increases with increasing energy. Of interest is the fact that decreasing the total

ionization cross section leads to increased N_2^+ 3914 emission. The reason for this is that the incident energy is now being deposited at lower altitudes, where the increased N_2 density offsets the decrease in ionization cross section.

Given that the solid and dashed lines in Figure 6 represent excellent agreement with both models and observations, the TST parameterization used here is clearly inappropriate for general aeronomic modeling purposes. This is not necessarily surprising, given that an auroral transport calculation is dependent on many cross sections which are interdependent [e.g. *Lummerzheim and Lilensten*, 1994] and in this study only one cross section was modified independently of all other elements. In spite of this, the modification was more than adequate for the purpose of establishing the relative uncertainties in a given calculation or between different models due to processes which affect the peak emission height of FUV emissions.

7. Conclusions

A sensitivity study of changes in derived auroral energy parameters to modifications of a key model cross section, the total N_2 ionization cross section, has been performed. The magnitude of the change in the total N_2 ionization cross section is large enough that this study covers the range of variations expected within a single model, or between two or more different models (see Figure 2). The current cross section parameterization used in AURCODE is referred to as GLR00 and the modified cross section is labeled TST. The conclusions are as follows.

1. Using the TST cross section decreases the altitude of modeled peak emissions relative to the GLR00 calculations (Figure 3) and decreases the peak emission rate. The

decrease in altitude is a function of incident energy with a 10 keV flux resulting in a decrease of approximately 3 km for a nominal 107 km peak height. There is no discernable change for a 500 eV flux.

2. The decrease in peak production height occurs within a region of very rapidly varying O_2 absorption (Figure 1). This translates into an energy-dependent change in modeled column intensities and their ratios. This change is shown to be primarily due to the change in peak emission height with the region of O_2 absorption and not from the slight decrease in peak production (Table 1). The magnitude of change increases with energy.

3. Using the TST cross section, the derived energy flux from UVI LBHL observations is approximately 16% smaller at 10 keV than that modeled with the GLR00 cross sections. Derived mean energies are also smaller with the TST cross section than with the GLR00 values. An emission ratio that results in a mean energy determination of 10 keV using the RT90 parameterization results in a mean energy of 7.7 keV using the TST values. This effect is smaller at lower incident energies.

4. The TST cross section parameterization significantly impacts other modeled aeronomic emissions and cannot be justified for general purpose calculations (Figure 6). This is not surprising given the limited nature of the modification and is unrelated to the primary purpose of this study.

5. In the course of this study, a coding error was found in the original RT90 cross section parameterization. However, the changes ascribed to this error have been shown to be approximately 6% or less for all cases. Thus previous studies should not be adversely affected by this discovery.

It is difficult to estimate the error contribution from the modeling process for derived energy parameters from FUV observations. However, this study serves as a proxy for one class of uncertainties—those that affect the modeled emission heights below 110 km. Since the perturbation used here is unrealistically large, the calculated errors can be taken as upper limits for uncertainties for this class of error either within a single model, or between different models.

References

Anderson, P.C., D.L. McKenzie, M.J. Brittnacher, M.W. Chen, M. Hairston, and M.F. Thomsen, Global storm time auroral X-ray morphology and timing and comparison with UV measurements, *J. Geophys. Res.*, *105*, 15,757-15,777, 2000.

Angelopoulos, V., T.D. Phan, D.E. Larson, F.S. Mozer, R.P. Lin, K. Tsuruda, T. Mukai, S. Kokubun, T. Yamamoto, D.J. Williams, R.W. McEntire, R.P. Lepping, G.K. Parks, M. Brittnacher, G. Germany, J. Spann, H.J. Singer, and K. Yumoto, Magnetottail flow bursts: Association to global magnetospheric circulation, relationship to ionospheric activity and direct evidence for localization, *Geophys. Res. Lett.*, *24*, 2271, 1997.

Borst, W.L., and E.C. Zipf, Cross section for electron-impact excitation of the (0,0) first negative band of N_2^+ from threshold to 2 keV, *Phys. Rev. A*, *1*, 834-840, 1970.

Brittnacher, M., M. Fillingim, G. Parks, G. Germany, and J. Spann, Polar cap area and boundary motion during substorms, *J. Geophys. Res.*, *104*, 12251-12262, 1999.

Chua, D., M. Brittnacher, G. Parks, G. Germany, and J. Spann, A new auroral feature: The nightside gap, *Geophys. Res. Lett.*, *25*, 3747, 1998.

Doe, R.A., J.D. Kelly, D. Lummerzheim, G.K. Parks, M.J. Brittnacher, G. Germany, and J. Spann, Initial comparison of POLAR UVI and Sondrestrom IS radar estimates for auroral electron energy flux, *Geophys. Res. Lett.*, *24*, 999, 1997.

Germany, G.A., G.K. Parks, M. Brittnacher, L. Chen, J.F. Spann, P.G. Richards, J. Cumnock, and F. Rich, Remote determination of auroral energy characteristics during substorm activity, *Geophys. Res. Lett.*, *24*, 995, 1997.

Germany, G.A., G.K. Parks, M.J. Brittnacher, J.F. Spann, J. Cumnock, D. Lummerzheim, F. Rich, and P.G. Richards, Energy characterization of a dynamic auroral event using GGS UVI images, in *Geospace Mass and Energy Flow: Results from the International Solar-Terrestrial Physics Program*, edited by J. Horwitz, D. Gallagher, and W. Peterson, pp. 143-148, AGU, 1998a.

Germany, G.A., G.K. Parks, H. Ranganath, R. Elsen, P.G. Richards, W. Swift, J.F. Spann, and M. Brittnacher, Analysis of auroral morphology: Substorm precursor and onset on January 10, 1997, *Geophys. Res. Lett.*, *25*, 3043, 1998b.

Germany, G.A., J.F. Spann, G.K. Parks, M.J. Brittnacher, R. Elsen, L. Chen, D. Lummerzheim, and M.H. Rees, Auroral Observations from the POLAR Ultraviolet Imager (UVI), in *Geospace Mass and Energy Flow: Results from the International Solar-Terrestrial Physics Program*, edited by J. Horwitz, D. Gallagher, and W. Peterson, AGU, 1998c.

Germany, G.A., D.G. Torr, P.G. Richards, M.R. Torr, and S. John, Determination of ionospheric conductivities from FUV auroral emissions, *J. Geophys. Res.*, *99*, 23297, 1994a.

Germany, G.A., M.R. Torr, P.G. Richards, and D.G. Torr, The dependence of modeled OI 1356 and N_2 LBH auroral emissions on the neutral atmosphere, *J. Geophys. Res.*, *95*, 7725, 1990.

Germany, G.A., M.R. Torr, D.G. Torr, and P.G. Richards, Use of FUV Auroral Emissions as Diagnostic Indicators, *J. Geophys. Res.*, *99*, 383, 1994b.

Kieffer, L.J., and G.H. Dunn, Electron impact ionization cross-section data for atoms, atomic ions, and diatomic molecules: I. Experimental data, *Rev. Mod. Phys.*, *38*, 1, 1966.

Liou, K., P.T. Newell, C.-I. Meng, A.T.Y. Lui, M. Brittnacher, and G. Parks, Synoptic auroral distribution: A survey using POLAR ultraviolet imagery, *J. Geophys. Res.*, *102*, 27197, 1997.

Lummerzheim, D., M. Brittnacher, D. Evans, G.A. Germany, G.K. Parks, M.H. Rees, and J.F. Spann, High time resolution study of the hemispheric energy flux carried by energetic electrons into the ionosphere during the May 19/20 auroral activity, *Geophys. Res. Lett.*, *24*, 987, 1997.

Lummerzheim, D., and J. Lilensten, Electron transport and energy degradation in the ionosphere: Evaluation of the numerical solution, comparison with laboratory experiments and auroral observations, *Ann. Geophys.*, *12*, 1039, 1994.

Lummerzheim, D., M.H. Rees, J.D. Craven, and L.A. Frank, Ionospheric conductances derived from DE-1 auroral images, *J. Atmos. Terr. Phys.*, *53*, 281, 1991.

Ostgaard, N., J. Stadsnes, J. Bjordal, G. Germany, R.R. Vondrak, D.L. Chenette, J.G. Pronko, and S.A. Cummer, Global energy input derived from UVI and PIXIE, *EOS Trans. AGU, Spring Meet. Suppl.*, *81*, S378, 2000.

Peticolas, L., and D. Lummerzheim, Time-dependent transport of field-aligned bursts of electrons in flickering aurora, *J. Geophys. Res.*, *105*, 12,895-12,906, 2000.

Rapp, D., and P. Englander-Golden, Total cross sections for ionization and attachment in gases by electron impact I. Positive ionization, *J. Chem. Phys.*, *43*, 1464, 1965.

Richards, P.G., and D.G. Torr, Auroral modeling of the 3371 A emission rate: dependence on characteristic electron energy, *J. Geophys. Res.*, *95*, 10,337, 1990.

Schram, B.L., F.J. de Heer, M.J. van der Wiel, and J. Kistemaker, *Physica*, *31*, 94, 1964.

Strickland, D.J., J.R. Jasperse, and J.A. Whalen, Dependence of auroral FUV emissions on the incident electron spectrum and neutral atmosphere, *J. Geophys. Res.*, *88*, 8051, 1983.

Strickland, D.J., and R.R. Meier, A photoelectron model for the rapid computation of atmospheric excitation rates, Naval Research Laboratory, Washington, DC, 1982.

Torr, M.R., D.G. Torr, M. Zukic, R.B. Johnson, J. Ajello, P. Banks, K. Clark, K. Cole, C. Keffer, G. Parks, B. Tsurutani, and J. Spann, A far ultraviolet imager for the International Solar-Terrestrial Physics mission, *Space Sci. Rev.*, *71*, 329-383, 1995.

Van Zyl, B., and W. Pendleton, Jr., N_2^+(X), N_2^+(A), and N_2^+(B) production in e+N_2 collisions, *J. Geophys. Res.*, *100*, 23755-23762, 1995.

Figure Captions

Figure 1. Column transmission to space (CTS), the fraction of photons from a given altitude that can be detected from space, as a function of altitude for 5 LBH bands. A vertical reference line is also provided at CTS=1. (a) Range of attenuation between 100 and 150 km. (b) Detail of changes in attenuation between 105 and 110 km.

Figure 2. Total ionization cross sections for N_2. Circles: Measurements of [*Rapp and Englander-Golden*, 1965]. Crosses: Measurements of [*Schram et al.*, 1964]. Dashed line: Compilation from [*Strickland and Meier*, 1982]. Solid line: Parameterization of [*Richards and Torr*, 1990], scaled downward by 12% as described in the text (GLR00). Triangles: Measurements of [*Borst and Zipf*, 1970], normalized to GLR00 at 1 keV. Dotted line: High energy modification to more closely match [*Schram et al.*, 1964] (TST). The error bar at 100 eV represents the range of values adapted from [*Van Zyl and Pendleton*, 1995] (one standard deviation); see text.

Figure 3. Production rates as a function of altitude for LBH and 1356 for incident Gaussian distributions with 10 keV mean energy and 1 mW m^{-2} energy flux. Solid line: GRL00; dashed line: TST.

Figure 4. Emission ratios for the UVI LBHL and LBHS filters.

Figure 5. Relative energy derived from Figure 4, compared to the GLR00 parameterization.

Figure 6. Common aeronomic emissions modeled with the three parameterizations discussed previously. Solid line: RT90, dashed line: GLR00, dotted line: TST

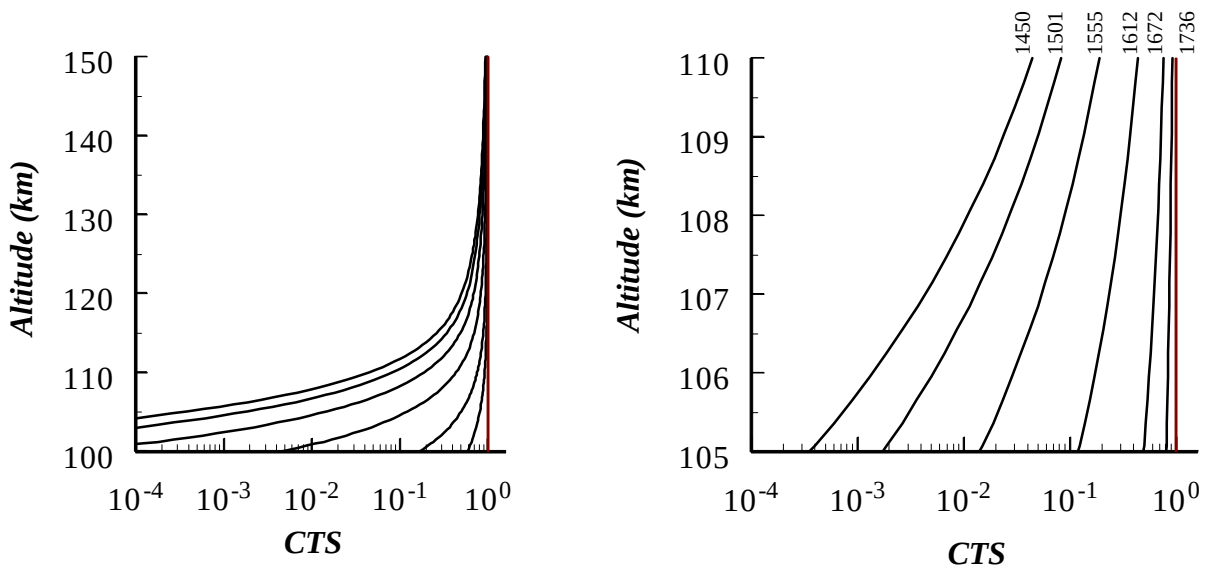

Figure 1. Column transmission to space (CTS), the fraction of photons from a given altitude that can be detected from space, as a function of altitude for 5 LBH bands. A vertical reference line is also provided at CTS=1. (a) Range of attenuation between 100 and 150 km. (b) Detail of changes in attenuation between 105 and 110 km.

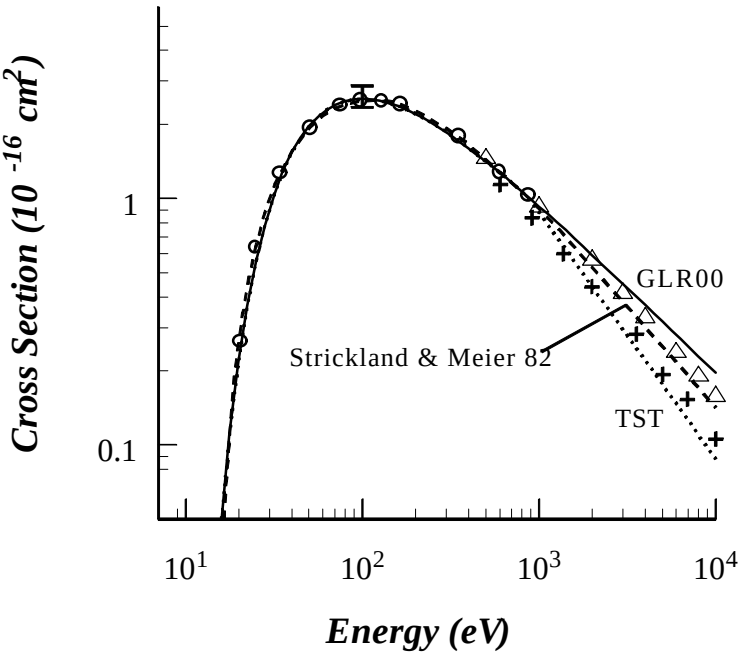

Figure 2. Total ionization cross sections for N_2. Circles: Measurements of [*Rapp and Englander-Golden,* 1965]. Crosses: Measurements of [*Schram et al.,* 1964]. Dashed line: Compilation from [*Strickland and Meier,* 1982]. Solid line: Parameterization of [*Richards and Torr,* 1990], scaled downward by 12% as described in the text (GLR00). Triangles: Measurements of [*Borst and Zipf*, 1970], normalized to GLR00 at 1 keV. Dotted line: High energy modification to more closely match [*Schram et al.*, 1964] (TST). The error bar at 100 eV represents the range of values adapted from [*Van Zyl and Pendleton*, 1995] (one standard deviation); see text.

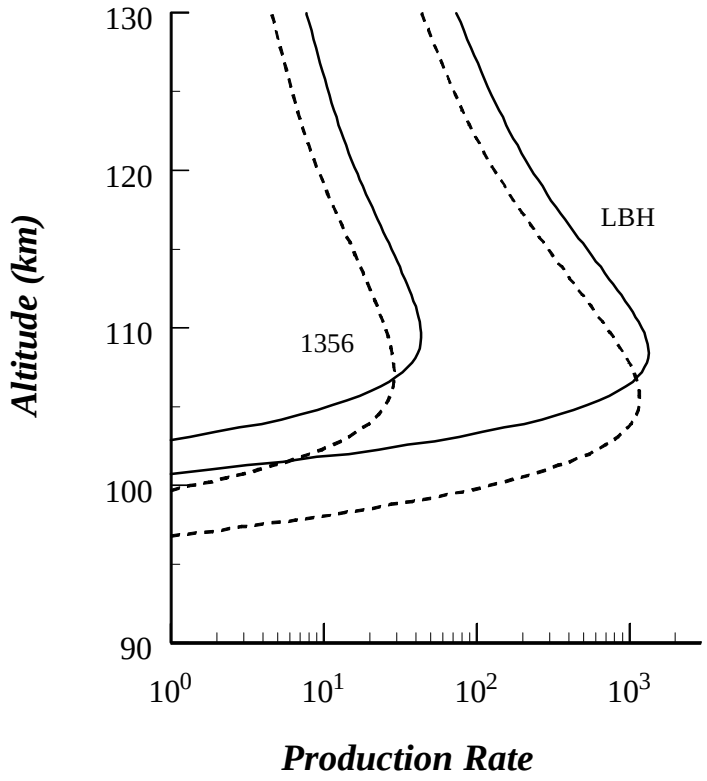

Figure 3. Production rates as a function of altitude for LBH and 1356 for incident Gaussian distributions with 10 keV mean energy and 1 mW m^{-2} energy flux. Solid line: GRL00; dashed line: TST.

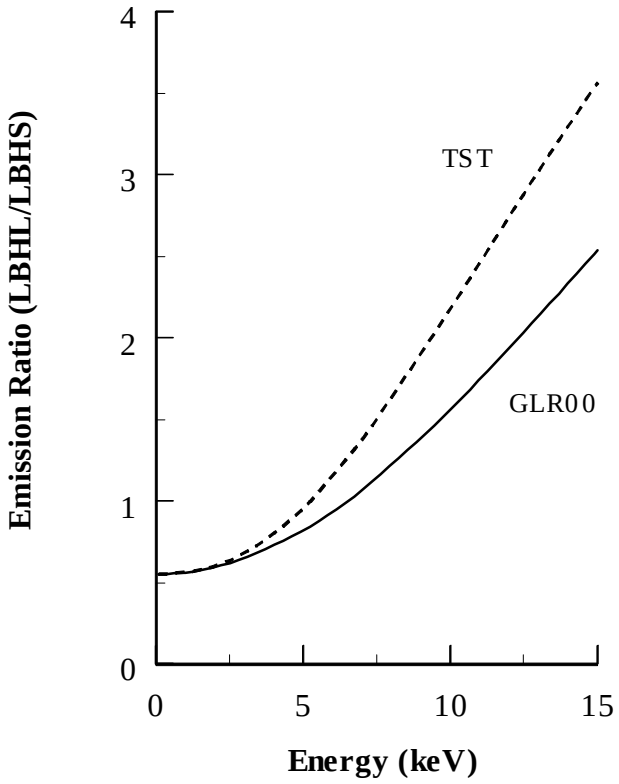

Figure 4. Emission ratios for the UVI LBHL and LBHS filters.

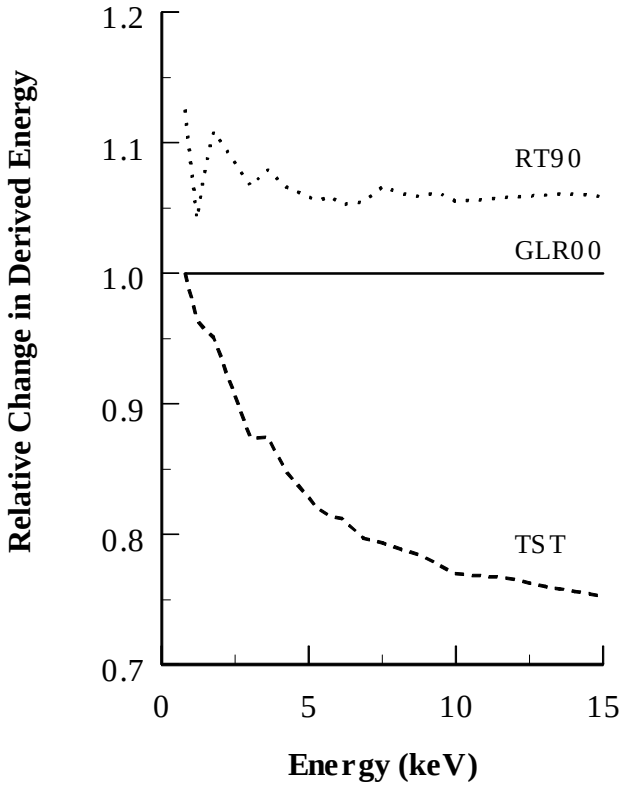

Figure 5. Relative energy derived from Figure 4, compared to the GLR00 parameterization.

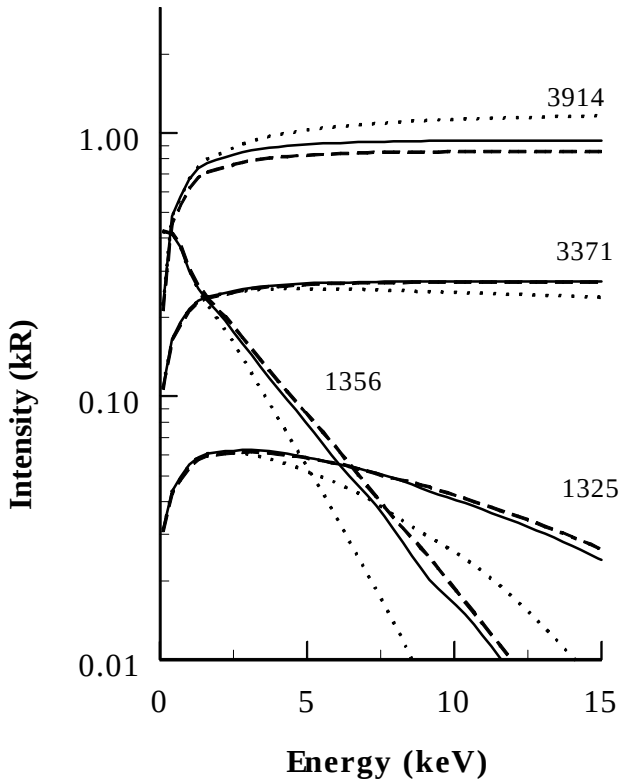

Figure 6. Common aeronomic emissions modeled with the three parameterizations discussed previously. Solid line: RT90, dashed line: GLR00, dotted line: TST

Table 1. Comparison of percent change in column brightness and peak emission rate for $O(^1S)$ 1356 and two LBH bands. The change is due to selecting between the GLR00 and TST parameterizations discussed in the text.

		With O_2 Absorption			Without O_2 Absorption		
	Energy (eV)	1356	LBH 1464	LBH 1838	1356	LBH 1464	LBH 1838
% change in Column Brightness	10k	70.7	41.4	8.8	28.2	9.4	8.8
% change in Peak Emission Rate	10k	33.3	13.0	12.5	33.3	13.0	12.5